

**Photoexcitation of astrophysically important states in  $^{26}\text{Mg}$** R. Longland,<sup>1,3</sup> C. Iliadis,<sup>1,3</sup> G. Rusev,<sup>2,3</sup> A. P. Tonchev,<sup>2,3</sup> R. J. deBoer,<sup>4</sup> J. Görres,<sup>4</sup> and M. Wiescher<sup>4</sup><sup>1</sup>*Department of Physics and Astronomy, University of North Carolina at Chapel Hill, Chapel Hill, North Carolina 27599, USA*<sup>2</sup>*Department of Physics, Duke University, Durham, North Carolina 27708, USA*<sup>3</sup>*Triangle Universities Nuclear Laboratory, Durham, North Carolina 27708, USA*<sup>4</sup>*Joint Institute for Nuclear Astrophysics, Department of Physics, University of Notre Dame, Notre Dame, Indiana 46556, USA*

(Received 4 August 2009; published 16 November 2009)

We performed a nuclear resonance fluorescence experiment to determine the energy and quantum numbers of excited states in  $^{26}\text{Mg}$ . Spin-parity ambiguities of excited states in  $^{26}\text{Mg}$ , the compound nucleus for the *s*-process neutron source  $^{22}\text{Ne}(\alpha,n)^{25}\text{Mg}$ , result in large uncertainties in the reaction rates. The present work uses the monoenergetic  $\gamma$ -ray beam from the High-Intensity  $\gamma$ -ray Source to probe states in the excitation energy range of  $E_x = 10.8$  to  $11.4$  MeV. Five excited states were observed and unambiguous quantum numbers were assigned at  $E_x = 10\,573.3(8)$  keV ( $J^\pi = 1^-$ ),  $E_x = 10\,647.3(8)$  keV ( $J^\pi = 1^+$ ),  $E_x = 10\,805.7(7)$  keV ( $J^\pi = 1^-$ ),  $E_x = 10\,949.1(8)$  keV ( $J^\pi = 1^-$ ), and  $E_x = 11\,153.5(10)$  keV ( $J^\pi = 1^+$ ). The two natural parity states, located between the  $\alpha$ -particle and neutron thresholds, are expected to significantly influence the rate of the competing  $^{22}\text{Ne}(\alpha,\gamma)^{26}\text{Mg}$  reaction. An important finding of this work is that the  $E_x = 11\,154$  keV level has unnatural parity, contrary to previous results, and thus does not contribute to the  $^{22}\text{Ne} + \alpha$  reaction rates.

DOI: [10.1103/PhysRevC.80.055803](https://doi.org/10.1103/PhysRevC.80.055803)

PACS number(s): 26.20.Kn, 21.10.Hw, 23.20.En, 27.30.+t

**I. INTRODUCTION**

The  $^{22}\text{Ne}(\alpha,n)^{25}\text{Mg}$  reaction is an important source of neutrons for the *s*-process in massive stars and asymptotic giant branch (AGB) stars. Massive stars are thought to produce the “weak component” of the *s*-process, increasing the abundance of lower mass nuclides. In AGB stars, the  $^{22}\text{Ne}(\alpha,n)^{25}\text{Mg}$  reaction works in conjunction with the  $^{13}\text{C}(\alpha,n)^{16}\text{O}$  reaction, producing the “main *s*-process component.” The former reaction sensitively influences branchings in the *s*-process path. Understanding the rate of the  $^{22}\text{Ne}(\alpha,n)^{25}\text{Mg}$  reaction and the competing  $^{22}\text{Ne}(\alpha,\gamma)^{26}\text{Mg}$  reaction is crucial for linking the observational evidence of *s*-process abundances with the internal structure of these stars.

At a typical temperature near  $T = 300$  MK, which is relevant for neutron production in massive stars and AGB stars, the Gamow peak for  $\alpha$ -particle capture on  $^{22}\text{Ne}$  occurs near  $E_0 = 600$  keV. At these low bombarding energies, the Coulomb barrier dominates the  $\alpha$ -particle partial width and, therefore, the reaction cross section decreases dramatically with decreasing energy. A consequence of the low cross section is that it is difficult to measure  $^{22}\text{Ne} + \alpha$  reactions directly. The lowest measured resonance is located at  $E_r(\text{lab}) = 830$  keV [1,2]. Thus, other methods must be utilized to obtain the properties of low-energy resonances to estimate reliable neutron production rates in stellar environments.

Prior to the present work, the nuclear properties of levels between the  $\alpha$ -particle threshold at  $S_\alpha = 10\,615$  keV and the lowest directly observed resonance ( $E_x = 11\,319$  keV) have been measured through neutron capture,  $\alpha$ -particle transfer, and photoneutron studies [3–8]. In addition to these works, nuclear resonance fluorescence (NRF) experiments using bremsstrahlung beams [9,10] and inelastic proton scattering experiments [11,12] have observed two states in the excitation energy region of interest at  $E_x = 10\,649$  keV ( $J^\pi = 1^+$ ) [9,10] and  $E_x = 11\,154$  keV ( $J = 1^{(+)}$ ) [10–12]. The resolution of Ref. [12] was approximately 60 keV, so the  $1^+$  state observed

in that experiment could therefore be attributed to a number of excited states in this energy region. Transfer measurements [ $^{22}\text{Ne}(\alpha,^6\text{Li},d)^{26}\text{Mg}$ ] [6,8] have also been used to study low spin states between the  $\alpha$ -particle and neutron thresholds in  $^{26}\text{Mg}$ . Alpha-particle transfer studies typically yield excitation energy uncertainties in excess of several keV and, furthermore, do not provide unambiguous quantum numbers for excited states. A  $^{26}\text{Mg}(\gamma,\gamma')^{26}\text{Mg}$  measurement with a polarized, monoenergetic  $\gamma$ -ray beam can be useful to significantly improve the uncertainties in the  $^{22}\text{Ne}(\alpha,\gamma)^{26}\text{Mg}$  and  $^{22}\text{Ne}(\alpha,n)^{25}\text{Mg}$  reaction rates. The High-Intensity  $\gamma$ -ray Source (HI $\gamma$ S) at the Triangle Universities Nuclear Laboratory (TUNL), utilizing a linearly polarised  $\gamma$ -ray beam, is perfectly suited for this purpose.

In this article we present the experimental results of the spin and parity measurements of dipole states in the  $^{26}\text{Mg}(\gamma,\gamma')^{26}\text{Mg}$  reaction. These measurements were made in the energy region important to astrophysical reaction rate calculations. The experimental setup is discussed in Sec. II and Sec. III outlines the theory needed to interpret  $\gamma$ -ray angular correlation measurements. The results of the experiment are presented in Sec. IV, a discussion follows in Sec. V, and conclusions are given in Sec. VI.

**II. EXPERIMENTAL SETUP****A. Photon beam**

The experiment was performed at the TUNL HI $\gamma$ S facility, where linearly polarized monoenergetic photon beams are produced by the intracavity Compton backscattering of laser photons from relativistic electrons in a storage ring. The storage ring of the HI $\gamma$ S facility was operated with two electron bunches at an energy of  $E_{e^-} = 515$ – $530$  MeV and a current of  $I_{e^-} \approx 45$  mA. We used a 1.91-cm collimator, which defined the diameter of the beam that was incident on the sample and

resulted in a beam energy spread of about 200 keV at a beam energy of 11.0 MeV. The intensity of the 100% linearly polarized photon beam at the sample was about  $10^7 \text{ s}^{-1}$ . Four incident  $\gamma$ -ray beam energies were used throughout the experiment: 10.8, 11.0, 11.2, and 11.4 MeV. A beam dump downstream from the sample reduced Compton scattering into the detectors. Further details of the HI $\gamma$ S facility can be found in Ref. [13].

### B. Samples

The sample consisted of magnesium-oxide (MgO) powder, enriched to 99.41(6)% in  $^{26}\text{Mg}$ . The  $^{24}\text{Mg}$  and  $^{25}\text{Mg}$  compositions were 0.41(2)% and 0.18(4)%, respectively. In addition, a spectroscopic analysis of the sample, performed at Oak Ridge National Laboratory who provided the sample, revealed only small impurities at concentrations in excess of 10 parts per million (with iron at 10 ppm and zinc at 20 ppm). Impurities at less than 10 ppm could not be detected in that analysis and are irrelevant for the present work. The total sample mass amounted to 16 418.5 mg, corresponding to a  $^{26}\text{Mg}$  mass of 10 162.5 mg. The sample was contained in a polycarbonate cylindrical container with 0.16-cm-thick walls and end caps, with an inner cavity 2.30 cm in diameter and 3.10 cm in length. In addition, a natural magnesium oxide ( $^{\text{nat}}\text{MgO}$ ) sample (79%  $^{24}\text{Mg}$ , 11%  $^{25}\text{Mg}$ , and 10%  $^{26}\text{Mg}$ ), housed in an identical polycarbonate container, was used for background measurements and energy calibrations. This  $^{\text{nat}}\text{MgO}$  sample had a mass of 4.3 g.

### C. Detectors

Four high-purity germanium (HPGe) detectors with relative efficiencies of 60% were used in the measurements. The detectors were arranged around the sample as shown in Fig. 1. Three detectors, two vertical and one horizontal, were positioned perpendicular to the incident beam, whereas one detector—the “out-of-plane” detector—was located outside the vertical plane. These positions were chosen to unambiguously determine the spins and parities of  $^{26}\text{Mg}$  excited states, as will be discussed in Sec. III.

Each detector was placed at a distance of about 10 cm from the center of the sample. After positioning, the  $\gamma$ -ray beam was aligned with a high-resolution beam imager to ensure homogeneous beam intensity across the sample. Small differences in detector geometry were later accounted for using Monte Carlo simulations (GEANT4 [14]) and radioactive source measurements. Each detector had a passive shield and absorber composed of lead and copper. The purpose of the absorbers was to reduce contributions from low-energy background and 511-keV annihilation  $\gamma$  rays produced in the sample.

## III. NUCLEAR RESONANCE FLUORESCENCE

A linearly polarized photon beam incident on a  $J^\pi = 0^+$  target nucleus such as  $^{26}\text{Mg}$  gives rise to a distinct radiation pattern depending on the quantum numbers of the excited states [15]. The observed intensity pattern is referred to as polarization-direction correlation. This type of angular correlation is described in detail in Ref. [16]. Our detector geometry

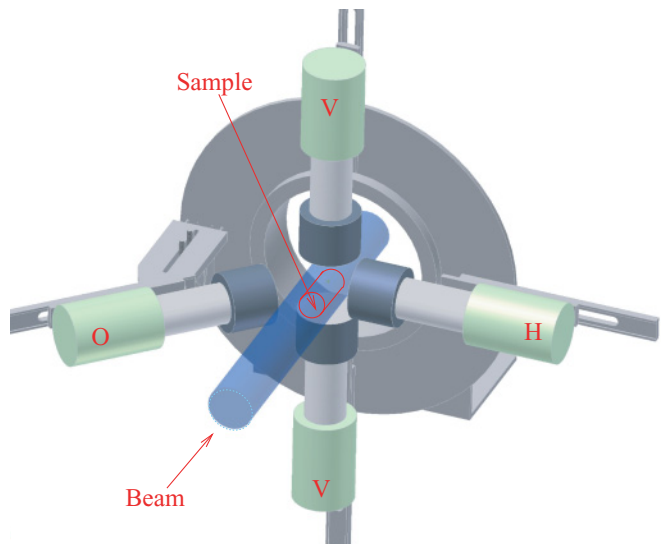


FIG. 1. (Color online) The detector setup used for energy and spin-parity measurements of  $^{26}\text{Mg}$  excited states. The sample was placed at the center of the array consisting of four 60% HPGe detectors where the labels V, H, and O represent the vertical, horizontal, and out-of-plane detectors, respectively. The dark gray cylinders shown on the front faces of the detectors are passive lead and copper shields. The detector labels correspond to the indices referred to in the text.

was similar to the one used in earlier experiments at the HI $\gamma$ S facility (see Ref. [13] and references therein). The only change we made was to move one of the horizontal detectors out of the vertical plane to a backward angle. This change was necessary to unambiguously distinguish between radiation from  $J = 1$  and  $J = 2$  excited states (see the following).

For an incident linearly polarized  $\gamma$ -ray beam, the angular correlation function, which is proportional to the probability of de-excitation in a particular direction, for pure transitions (i.e., those involving unique quantum numbers) is given by [16]

$$\begin{aligned}
 W_{\text{theory}}(\theta, \phi) &= \sum_n F_n(L_1, L_1, j_1, j) F_n(L_2, L_2, j_2, j) \\
 &\times \left\{ P_n(\cos \theta) + (-1)^{\sigma_1} \frac{\langle L_1 1 L_1 1 | n 2 \rangle}{\langle L_1 1 L_1 - 1 | n 0 \rangle} \right. \\
 &\times \left. \left( \frac{(n-2)!}{(n+2)!} \right)^{1/2} \cos(2\phi) P_n^{(2)}(\cos \theta) \right\}, \\
 F_n(L_a, L'_a, j_a, j) &= (-1)^{j_a - j - 1} \sqrt{(2j+1)(2L_a+1)(2L'_a)} \\
 &\times \langle L_a 1 L'_a - 1 | n 0 \rangle W(j j L_a L'_a; n j_a),
 \end{aligned} \tag{1}$$

where  $n$  is an even integer ranging from 0 to  $n_{\text{max}} = \min(2j+1, 2L_1+1, 2L_2+1)$ , where the subscripts 1 and 2 refer to the first (incident beam) and second (detected radiation) radiations (where the incident beam has known polarization);  $\langle L_a 1 L'_a - 1 | n 0 \rangle$  is a Clebsch-Gordan coefficient;  $W(j j L_a L'_a; n j_a)$  is a Racah coefficient;  $P_n(\cos \theta)$  is an  $n$ th-order Legendre polynomial;  $P_n^{(2)}(\cos \theta)$  is an  $n$ th-order associated Legendre polynomial;  $j_1$ ,  $j$ , and  $j_2$  correspond to

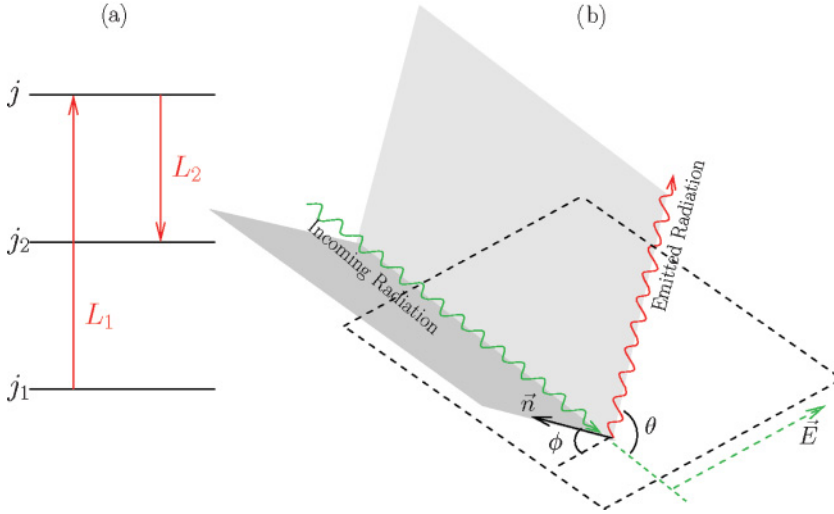


FIG. 2. (Color online) (a) Sample level scheme, showing excitation and de-excitation of a nucleus. (b) Definition of the coordinate system used in Eq. (1). The angle  $\theta$  is defined as the angle between the emitted radiation and the incoming  $\gamma$ -ray beam. The angle  $\phi$  is the angle between the polarization plane of the incoming  $\gamma$ -ray beam and the plane defined by the direction of the incoming  $\gamma$ -ray beam and the normal to the plane defined by the incoming  $\gamma$ -ray beam and the emitted radiation direction. For example, if the emitted  $\gamma$  ray is detected in a counter located in the horizontal plane,  $\phi = 90^\circ$ .

the initial, intermediate, and final state spins, respectively;  $L_1$  and  $L_2$  are the excitation and de-excitation  $\gamma$ -ray multipolarities, respectively; and  $\sigma_1 = 0$  for electric transitions and 1 for magnetic transitions. The angles in Eq. (1) are defined as follows: (i)  $\theta$  is the angle of the emitted radiation with respect to the incoming polarized  $\gamma$ -ray beam. (ii)  $\phi$  is the angle between the polarization plane of the incoming radiation (the horizontal plane in our experiment) and the plane defined by the direction of the incoming  $\gamma$ -ray beam and the normal to the plane defined by the incoming  $\gamma$ -ray beam and the emitted radiation direction. A sample decay scheme and the angles  $\theta$  and  $\phi$  are shown in Fig. 2.

The angular correlations for the most important spin sequences of relevance to the present work are given by

$$\begin{aligned} 0^+ \rightarrow 1^\pm \rightarrow 0^+ : \quad & W_{\text{theory}}(\theta, \phi) \\ &= 1 + \frac{1}{2} \left\{ P_2(\cos \theta) + \frac{1}{2} (-1)^{\sigma_1} P_2^{(2)}(\cos \theta) \cos(2\phi) \right\}, \end{aligned} \quad (2)$$

$$\begin{aligned} 0^+ \rightarrow 2^\pm \rightarrow 0^+ : \quad & W_{\text{theory}}(\theta, \phi) \\ &= 1 + \left\{ \frac{5}{14} P_2(\cos \theta) + \frac{8}{7} P_4(\cos \theta) \right\} - (-1)^{\sigma_1} \\ &\quad \times \left\{ \frac{5}{28} P_2^{(2)}(\cos \theta) - \frac{2}{21} P_4^{(2)}(\cos \theta) \right\} \cos(2\phi), \end{aligned} \quad (3)$$

$$\begin{aligned} 0^+ \rightarrow 1^\pm \rightarrow 2^+ : \quad & W_{\text{theory}}(\theta, \phi) \\ &= 1 + \frac{1}{20} \left\{ \frac{1}{10} P_2(\cos \theta) + \frac{1}{\sqrt{2}} (-1)^{\sigma_1} \right. \\ &\quad \left. \times P_2^{(2)}(\cos \theta) \cos(2\phi) \right\}, \end{aligned} \quad (4)$$

where the three  $J^\pi$  values refer to the sample ground state ( $0^+$ ), the intermediate excited state, and the final state, respectively.

For the detector positions shown in Fig. 2, Eqs. (2)–(4) yield values for  $W_{\text{theory}}(\theta, \phi)$  that are listed in Table I. Finite solid angle effects were accounted for using Monte Carlo simulations. The adjusted and experimentally expected angular correlations  $W_{\text{adj}}(\theta, \phi)$  are also listed in Table I.

To better visualise the angular correlations, expected radiation patterns for sample spin sequences are shown in Fig. 3. We first consider the sequence  $0^+ \rightarrow 1^- \rightarrow 0^+$ , shown in the upper left panel of Fig. 3. No intensity is observed by the horizontal detector (H), maximum intensity is observed by the vertical detector (V), and some intensity is observed by the out-of-plane detector (O). A very different radiation pattern is observed for the spin sequence  $0^+ \rightarrow 1^+ \rightarrow 0^+$  (upper right panel), for which maximum intensity is observed in both the horizontal and out-of-plane detectors, and no intensity is observed in the vertical detector. Considering now the  $0^+ \rightarrow 2^+ \rightarrow 0^+$  sequence (lower left panel), we find that the vertical and horizontal detectors observe the same intensity ratios as for the  $0^+ \rightarrow 1^+ \rightarrow 0^+$  spin sequence, and thus we cannot distinguish between the excitation of a  $J^\pi = 1^+$  or  $2^+$  intermediate state based on these two detectors alone. This is why a detector was placed out of the vertical plane—it detects no intensity for a  $2^+$  intermediate state, whereas it detects maximum intensity for a  $1^+$  intermediate state. The radiation patterns are distinct and lead to unambiguous spin-parity assignments for the intermediate (excited  $^{26}\text{Mg}$ ) state.

TABLE I. Angular correlations for spin sequences that are relevant to the present analysis. The detectors were positioned as follows: The horizontal detector H was at  $(\theta, \phi) = (90^\circ, 90^\circ)$ , the two vertical detectors V were at  $(\theta, \phi) = (90^\circ, 0^\circ)$ , and the out-of-plane detector O was at  $(\theta, \phi) = (135^\circ, 90^\circ)$  (see Fig. 2). Columns 2, 3, and 4 list the theoretical angular correlations, calculated using Eq. (1). Columns 5, 6, and 7 show the adjusted angular correlations,  $W_{\text{adj}}(\theta, \phi)$ , accounting for finite detector and sample solid angle effects.

Sequence	$W_{\text{theory}}(\theta, \phi)$			$W_{\text{adj}}(\theta, \phi)$		
	H	V	O	H	V	O
$0^+ \rightarrow 1^+ \rightarrow 0^+$	1.5	0	1.5	1.47	0.04	1.47
$0^+ \rightarrow 1^- \rightarrow 0^+$	0	1.5	0.75	0.04	1.47	0.75
$0^+ \rightarrow 2^+ \rightarrow 0^+$	2.5	0	0	2.36	0.07	0.08
$0^+ \rightarrow 2^- \rightarrow 0^+$	0	2.5	1.25	0.06	2.31	1.22
$0^+ \rightarrow 1^+ \rightarrow 2^+$	1.05	0.9	1.05	1.05	0.90	1.05
$0^+ \rightarrow 1^- \rightarrow 2^+$	0.9	1.05	0.975	0.90	1.05	0.97

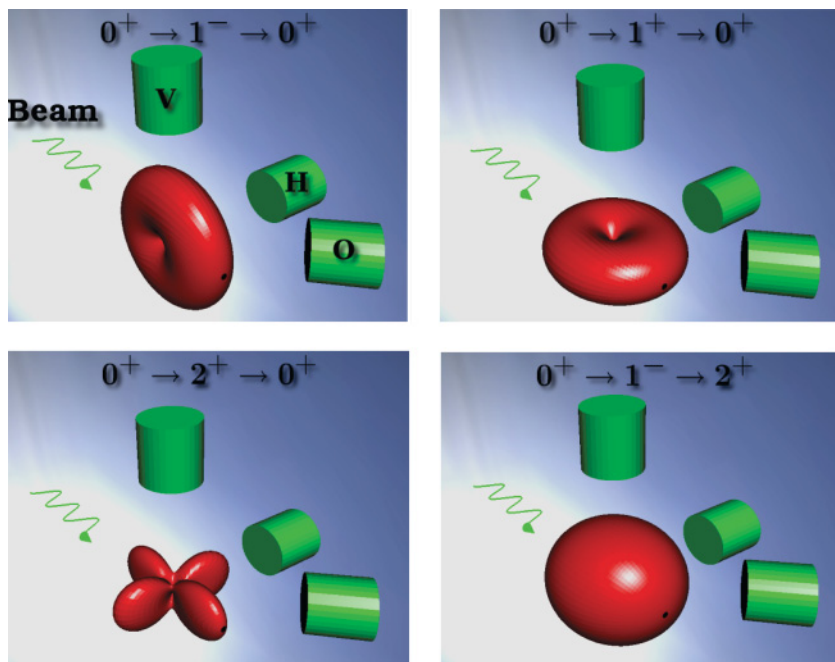


FIG. 3. (Color online) The angular correlation distributions for sample spin sequences  $0^+ \rightarrow 1^- \rightarrow 0^+$ ,  $0^+ \rightarrow 1^+ \rightarrow 0^+$ ,  $0^+ \rightarrow 2^+ \rightarrow 0^+$ , and  $0^+ \rightarrow 1^- \rightarrow 2^+$ . The labels refer to the detector position (V is vertical plane, H is horizontal plane, and O is out-of-plane). For reasons of clarity, the out-of-plane detector is shown at  $\theta = 45^\circ$  rather than  $\theta = 135^\circ$  (since the distributions are symmetric around  $\theta = 90^\circ$ ).

#### IV. PROCEDURE AND RESULTS

Incident beam energies of  $E_\gamma = 10.8, 11.0, 11.2,$  and  $11.4$  MeV were used to populate excited states in  $^{26}\text{Mg}$ . For each energy, the beam was incident on the sample for approximately 11 hours. The beam energy spread had a full width at half maximum of about 2%, corresponding to 200 keV at  $E_\gamma = 11.0$  MeV. This resolution was determined by first inserting beam attenuators into the  $\gamma$ -ray beam to reduce the flux to acceptable limits, and then inserting an HPGc detector. The beam energy spread could be extracted from the high-energy part of the detected spectrum, which was least affected by the detector response (i.e., from Compton scattered events and pair-production  $\gamma$  rays).

Spectra using  $^{\text{nat}}\text{Mg}$  were recorded at the same incident  $\gamma$ -ray beam energies as for the  $^{26}\text{MgO}$  sample, but for only half of the acquisition time. The spectra are important for two reasons: (i) for background peak identification from sample impurities, particularly from  $^{24}\text{Mg}$ , as well as from the container; and (ii) for the detector energy calibration. The background runs helped us to unambiguously assign observed transitions to  $^{26}\text{Mg}$ . The energy calibration was performed by populating the well-known  $^{24}\text{Mg}$  excited state at  $E_x = 9967.8(3)$  keV, which decays to the first excited state at  $E_x = 1368.675(6)$  keV [17] with the emission of nearly isotropic radiation. The measured energy must be corrected for the recoil shift in all three detectors, as well as for the Doppler shift in the out-of-plane detector (at  $\theta = 135^\circ$ ). Well-known room background lines below 3 MeV ( $^{40}\text{K}$  and  $^{208}\text{Tl}$ ) were also used in the energy calibration. Excitation energies of  $^{26}\text{Mg}$  states were determined from the observed de-excitation  $\gamma$  rays to both ground and excited states, after correction for recoil and Doppler shift. A weighted average of the excitation energies obtained from all detectors was performed. The uncertainties in the observed  $\gamma$ -ray energies arise from statistical uncertainties and uncertainties in the

energy calibration. Table II presents a comparison between the present excitation energies and the literature values. We find that the the new  $E_x$  values agree with previous results, but the uncertainties are significantly smaller.

Detector efficiencies must be known to obtain spin-parity assignments and decay branching ratios. A combination of radioactive source measurements and Monte Carlo simulations was used to obtain the full-energy peak efficiencies of the detectors. (Escape peaks were not used in the analysis.) The radioactive sources used were  $^{60}\text{Co}$  and  $^{56}\text{Co}$ , which yield efficiencies up to about  $E_\gamma = 3.5$  MeV. The sum-peak method [19] was used with  $^{60}\text{Co}$  to obtain absolute efficiencies, independent of source activities. The  $^{56}\text{Co}$  full-energy peak efficiencies could then be normalized to the  $^{60}\text{Co}$  absolute efficiency measurements. Monte Carlo simulations were then used to extrapolate full-energy peak efficiencies to the higher energies covered in the present experiment. The effect of atomic absorption of  $\gamma$  rays in the sample was accounted for in the simulations by treating the MgO as an extended sample. Detection efficiencies for individual full-energy peaks were obtained by cubic spline interpolation between simulated full-energy peak efficiencies. The uncertainty of full-energy peak

TABLE II. Excitation energies in  $^{26}\text{Mg}$  (in KeV) for states populated in the present experiment. Also shown are the excitation energies obtained from the literature. Excitation energies from Ref. [18] are compiled from external sources.

Present	[18]	[7]	[8]	[10]
10573.3(8)	10567(3)			
10647.3(8)	10646(2)			10648.8(5)
10805.7(7)	10805.9(4)		10808(20)	
10949.1(8)	10945(3)		10953(25)	
11153.5(10)	11153.2(2)	11153.386(86)		11153.8(12)

TABLE III. Observed ground-state transition intensities (efficiency corrected) and resulting quantum numbers for excited states in  $^{26}\text{Mg}$ .  $I_H$ ,  $I_V$ , and  $I_O$  refer to the relative intensity (normalized to the angular correlations) observed in the horizontal, vertical and out-of-plane detectors, respectively; the label N refers to natural parity (i.e.,  $J^\pi = 0^+, 1^-, 2^+, \dots$ ). The upper limits listed here correspond to 90% Gaussian confidence limits.

$E_x$	Present results				$J^\pi$	Literature $J^\pi$ assignments			
	$I_H$	$I_V$	$I_O$			[18]	[4]	[8]	[10]
10573	$\leq 1.2$	1.47(3)	$\leq 1.3$		$1^-$				
10647	1.45(3)	0.044(9)	1.47(3)		$1^+$	$1^+$			$1^+$
10805	$\leq 0.5$	1.47(4)	$\leq 0.9$		$1^-$	$(0^+ - 4^+)$		N	
10949	$\leq 0.4$	1.47(1)	0.6(3)		$1^-$		(4-7)	N	
11154	1.47(9)	0.015(7)	1.44(9)		$1^+$	$1^-$			1

efficiencies near  $E_\gamma = 11$  MeV, arising from uncertainties in both detector geometry and other experimental uncertainties, was assumed to be 5%.

Quantum numbers of the observed states were assigned by considering the observed radiation pattern. Note that we observe intensity at the locations where the theoretical angular correlation  $W(\theta, \phi)$  is zero because of finite solid angle effects. Such effects were modeled using Monte Carlo simulations and could be accounted for. For each ground-state transition, the efficiency-corrected measured full-energy peak intensities normalized to the theoretical angular correlations are shown in Table III. Comparison to the  $W_{\text{adj}}(\theta, \phi)$  values listed in Table I was performed by normalizing the highest observed intensity to the adjusted theoretical angular correlation expected from the given detector. The normalization was performed in this way because  $W_{\text{adj}}(\theta, \phi)$  describes the theoretical scaling of detected intensities between detectors for a chosen spin sequence. After normalization, comparison of observed intensities with the theoretical angular correlations in Table I immediately reveals the spin sequence that gives rise to the observed intensities. These comparisons are shown in Fig. 4 for four of the ground-state transitions listed in Table III. Our unambiguous

$J^\pi$  assignments are consistent with previous  $J^\pi$  assignments or restrictions, except for a single case (see following). Branching ratios were calculated from the observed peak intensities and corrected for angular correlations and detector efficiencies. Table IV shows the branching ratios observed in our experiment. Our observed branching ratios agree with previous measurements [5,9], with one exception, which is discussed later. In addition, the relatively low background from the monoenergetic  $\gamma$ -ray beam has allowed us to resolve additional, weaker decay branches in populated states. Decay widths will be published in a forthcoming paper.

Sample spectra, which were measured at a beam energy of 11.2 MeV for approximately 11 h, are shown in Fig. 5. The decay of the two states at  $E_x = 11154$  keV and  $E_x = 10949$  keV is observed; these will be used to illustrate the assignment of quantum numbers to excited states. Decay of the populated state at  $E_x = 11154$  keV to the ground state ( $0^+$ ) is observed as well as to the excited state at  $E_x = 3589$  keV ( $0^+$ ). Approximately equal intensity (after proper efficiency corrections) is found in the horizontal and out-of-plane detectors, and no intensity is found in the vertical detectors. According to the expected angular correlations,

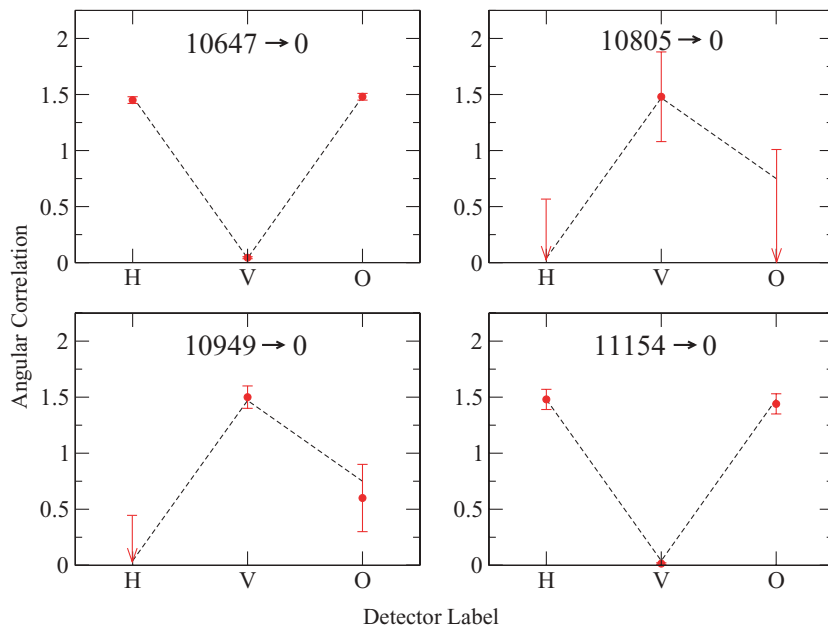


FIG. 4. (Color online) Efficiency-corrected, measured intensities (circles) for the four ground-state transitions listed in Table III compared to the adjusted theoretical angular distributions (dashed lines) from columns 5, 6, and 7 in Table I for the assigned spin-parities. The measured intensities are normalized so that the highest intensity for each transition equals the maximum adjusted theoretical angular correlation. Upper limit assignments are indicated with arrows.

TABLE IV. Observed branching ratios from populated excited states in  $^{26}\text{Mg}$ . The initial excitation energy  $E_{x_i}$ , the spin-parity  $J_i^\pi$ , and the branching ratio  $B_\gamma$  are from the present work. The final excitation energy  $E_{x_f}$  and the spin-parity  $J_f^\pi$  are from Ref. [17].

$E_{x_f}$ (keV)	$J_f^\pi$	Initial excited state, $E_{x_i}$ (keV), $J_i^\pi$				
		10573 1 <sup>-</sup>	10647 1 <sup>+</sup>	10806 1 <sup>-</sup>	10949 1 <sup>-</sup>	11154 1 <sup>+</sup>
0	0 <sup>+</sup>	0.47(10)	0.876(27)	0.218(61)	0.138(19)	0.688(81)
1809	2 <sup>+</sup>		0.0155(18)	0.782(87)	0.572(29)	0.029(4)
2938	2 <sup>+</sup>		0.0636(30)		0.135(13)	
3589	0 <sup>+</sup>				0.047(7)	0.110(22)
4333	2 <sup>+</sup>				0.108(96)	0.077(11)
4972	0 <sup>+</sup>	0.528(91)	0.0162(13)			0.096(24)
5292	2 <sup>+</sup>		0.0163(13)			
7100	2 <sup>+</sup>		0.0124(12)			

summarized in Table I and shown in Fig. 3, both of these observed  $\gamma$  rays must arise from a  $0^+ \rightarrow 1^+ \rightarrow 0^+$  spin sequence, so the state is assigned to  $J^\pi = 1^+$ . Decay from the  $E_x = 10949$  keV excited state to the first excited state at  $E_x = 1809$  keV ( $J^\pi = 2^+$ ) can also be seen in Fig. 5. This decay is observed with similar intensity in all detectors. The radiation pattern is consistent with an expected pattern for a  $0^+ \rightarrow 1^- \rightarrow 2^+$  spin sequence (Table I and Fig. 3). Thus, this state can be unambiguously assigned a spin parity of  $J^\pi = 1^-$ .

## V. DISCUSSION

Five excited states were observed in this experiment. The relatively low beam-induced background at the HI $\gamma$ S facility, coupled with good separation of states, allowed us to observe very weak branching ratios (Table IV) and make

unambiguous quantum number assignments for every excited state observed in our study. Previously, two of the states had unknown quantum numbers and large energy uncertainties. These energies have now been determined with significantly improved precision. One additional state was previously assigned quantum numbers that the current results show are incorrect. A detailed discussion of individual states follows.

The state observed at  $E_x = 10573$  keV has previously been observed at  $E_x = 10567(3)$  keV in inelastic proton scattering [11]. The quantum numbers of the state are determined to be  $J^\pi = 1^-$  in the present experiment, whereas none were assigned previously. Branching to the ground-state transition and the excited state at  $E_x = 4972$  keV were observed in the present work.

The state at  $E_x = 10647$  keV has previously been observed at  $E_x = 10646(2)$  keV with  $J^\pi = 1^+$  and a mean lifetime of  $\tau_m = 110(30)$  as [18], and by Ref. [10] at

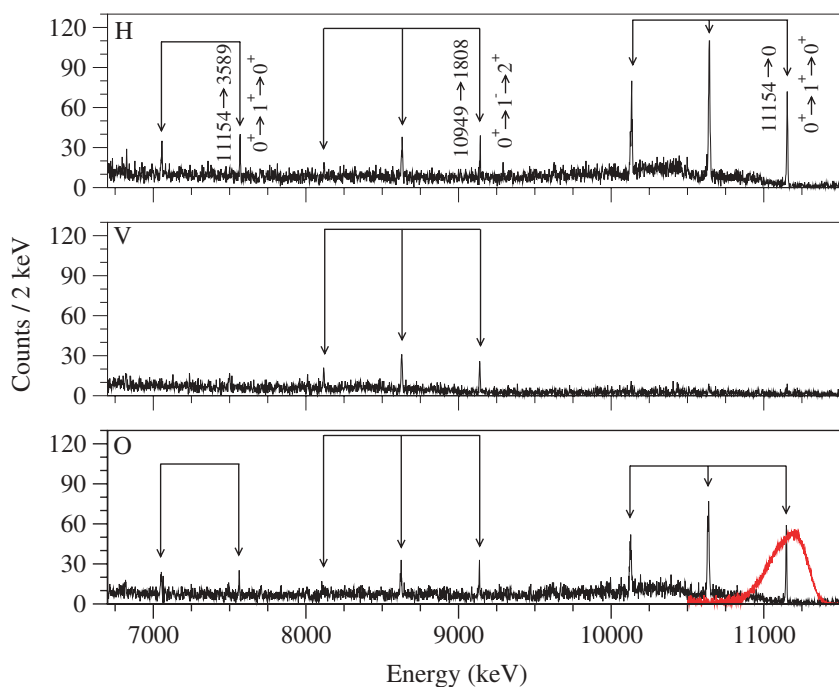


FIG. 5. (Color online) Spectra observed using the horizontal (H), vertical (V), and out-of-plane (O) detectors with a  $\gamma$ -ray beam energy of  $E_\gamma = 11.2$  MeV. Decays to the ground state and excited states are shown from the  $E_x = 11154$  keV ( $1^+$ ) and  $E_x = 10949$  keV ( $1^-$ ) states. The broad peak in the lower panel is the beam profile obtained from the zero-degree detector (arbitrary scale). See text for more discussion.

$E_x = 10\,648.8(5)$  keV. The current analysis agrees with the energy and quantum number assignments for this state. Only the ground-state transition has previously been measured by Berg *et al.* [9]. In total, we resolve five decays from this level, the strongest of which is the ground-state transition, with a branching ratio of 87.6(27)%.

The state at  $E_x = 10\,806$  keV has previously been observed in a thermal neutron capture experiment on  $^{25}\text{Mg}$  at  $E_x = 10\,805.9(4)$  keV [5] and through  $\alpha$ -particle transfer measurements on  $^{22}\text{Ne}$  at  $E_x = 10\,808(20)$  keV [8]. The neutron capture experiment placed restrictions on the quantum numbers of this state by observing the decay to the first excited state. The  $\alpha$ -particle transfer assigned natural parity. In the present work, we obtain an unambiguous  $J^\pi = 1^-$  assignment, consistent with the literature restrictions. The observed decay scheme agrees with that of Ref. [5] but resolves an additional weak branch to the ground state.

Levels near the  $E_x = 10\,950$  keV state have previously been observed in three experiments:  $^{26}\text{Mg}(p, p')^{26}\text{Mg}$  at  $E_x = 10\,950$  keV [11],  $^{22}\text{Ne}(^6\text{Li}, d)^{26}\text{Mg}$  at  $E_x = 10\,953(25)$  keV [8], and  $^{23}\text{Na}(\alpha, p\gamma)^{26}\text{Mg}$  at  $E_x = 10\,943(2)$  keV [4]. The current unambiguous assignment of  $J^\pi = 1^-$  is consistent with the natural parity assignment made in the  $\alpha$ -particle transfer measurement but is inconsistent with the decay observed in Ref. [4]. That work reports secondary decays to  $E_x = 7953$  keV ( $J^\pi = 5^-$ ) with a branching ratio of 64.5% and to  $E_x = 9169$  keV ( $J^\pi = 6^-$ ) with a branching ratio of 36.5%. Empirical rules [17] lead to  $J^\pi = (4^+ - 7^-)$  for the decaying state. Giesen *et al.* [6] also observed a state at 10.95 MeV and assigned it as  $J^\pi = (2^+, 3^-, 4^+)$ . The most likely explanation for the disagreement with our  $J^\pi$  assignment is the presence of a doublet at this energy, as suggested in Ref. [8]. Since there is not enough information to determine which of these states has the large  $\alpha$ -particle width seen by Ref. [8], we recommend that future  $^{22}\text{Ne} + \alpha$  thermonuclear reaction rate calculations be performed using the observed  $\alpha$ -particle width as an upper limit for both states.

The excited state observed at  $E_x = 11\,154$  keV corresponds to a  $^{22}\text{Ne}(\alpha, n)^{25}\text{Mg}$  resonance at  $E_r(\text{lab}) \approx 630$  keV, believed to have been seen in Refs. [20,21], but later proven to be caused by background from  $^{11}\text{B}$  [22]. An expected resonance at this location has since been treated as the most important expected contribution to the  $^{22}\text{Ne}(\alpha, n)^{25}\text{Mg}$  reaction rate and has been searched for repeatedly [2,6,8,22]. A state near this energy has also been observed through inelastic proton scattering at  $E_x = 11\,156$  keV [11] and  $E_x = 11\,150$  keV [12], photoneutron studies at  $E_x = 11\,153.8$  keV [3], neutron capture on  $^{25}\text{Mg}$  at  $E_x = 11\,153.387(86)$  keV [7], and photoexcitation experiments [9,10]. The proton scattering experiment of Ref. [11] and photoexcitation experiments did not assign quantum numbers, but the work of Ref. [3] suggested a spin-parity of  $J^\pi = 1^-$ , and Ref. [12] made a spin-parity

assignment of  $J^\pi = 1^+$ . However, excitation energy uncertainties of about 60 keV in that experiment lead to ambiguity regarding which excited state was observed. In the current work, this state was observed with very good statistics and energy resolution, as shown in Fig. 5. Our angular correlation measurements using the 100% linearly polarized photon beam unambiguously assigns  $J^\pi = 1^+$  to this level. This finding is significant since it rules out any contributions of this unnatural parity level to the  $^{22}\text{Ne} + \alpha$  reaction rates. No branchings to secondary excited states were observed in other experiments. We observed a total of four branchings (Table IV).

## VI. CONCLUSION

The  $^{22}\text{Ne}(\alpha, \gamma)^{26}\text{Mg}$  and  $^{22}\text{Ne}(\alpha, n)^{25}\text{Mg}$  reactions, which are important for s-process neutron production, proceed through excited states in the compound nucleus  $^{26}\text{Mg}$ . The important excitation energy region in  $^{26}\text{Mg}$ , corresponding to relevant resonances in the  $^{22}\text{Ne} + \alpha$  reaction, ranges from the  $\alpha$ -particle threshold at  $S_\alpha = 10\,615$  keV to  $E_x \approx 11\,600$  keV. Many of the states in this energy range have uncertain excitation energies and quantum numbers, which are essential ingredients for reaction rate calculations.

A  $^{26}\text{Mg}(\gamma, \gamma')^{26}\text{Mg}$  experiment was performed at the HI $\gamma$ S facility with  $\gamma$ -ray beam energies of  $E_\gamma = 10.8, 11.0, 11.2,$  and  $11.4$  MeV to determine the excited state quantum numbers for  $^{26}\text{Mg}$ . In total, five excited states were identified, with  $E_x = 10\,573.3(8)$  keV ( $J^\pi = 1^-$ ),  $E_x = 10\,647.3(8)$  keV ( $J^\pi = 1^+$ ),  $E_x = 10\,805.7(7)$  keV ( $J^\pi = 1^-$ ),  $E_x = 10\,949.1(8)$  keV ( $J^\pi = 1^-$ ), and  $E_x = 11\,153.5(10)$  keV ( $J^\pi = 1^+$ ). The excited states at  $E_x = 10\,806$  keV and  $E_x = 10\,949$  keV have previously been observed in  $\alpha$ -particle transfer studies with undetermined quantum numbers. The present results for these states, which are located below the neutron threshold, are expected to significantly influence the  $^{22}\text{Ne}(\alpha, \gamma)^{26}\text{Mg}$  reaction rate. The unnatural parity state observed at  $E_x = 11\,154$  keV was previously believed to be an important resonance in the  $^{22}\text{Ne} + \alpha$  reactions. However, the present results show that this state is irrelevant for neutron production in the s-process.

## ACKNOWLEDGMENTS

The authors would like to thank A. E. Champagne, J. R. Newton, S. Daigle, J. Cesaratto, and J. Kelly for their invaluable help with the experiment. This work was supported in part by the US Department of Energy under Contract Nos. DE-FG02-97ER41041 and DE-FG02-97ER41033 and by the Joint Institute for Nuclear Astrophysics NSF Grant No. PHYS 08-22648.

- 
- [1] K. Wolke, V. Harms, H. W. Becker, J. W. Hammer, K. L. Kratz, C. Rolfs, U. Schröder, H. P. Trautvetter, M. Wiescher, and A. Wöhr, *Z. Phys. A* **334**, 491 (1989).  
 [2] M. Jaeger, R. Kunz, A. Mayer, J. W. Hammer, G. Staudt, K. L. Kratz, and B. Pfeiffer, *Phys. Rev. Lett.* **87**, 202501 (2001).

- [3] B. L. Berman, R. L. van Hemert, and C. D. Bowman, *Phys. Rev. Lett.* **23**, 386 (1969).  
 [4] F. Glatz *et al.*, *Z. Phys. A* **324**, 187 (1986).  
 [5] T. A. Walkiewicz, S. Raman, E. T. Jurney, J. W. Starnner, and J. E. Lynn, *Phys. Rev. C* **45**, 1597 (1992).

- [6] U. Giesen *et al.*, Nucl. Phys. **A561**, 95 (1993).
- [7] P. E. Koehler, Phys. Rev. C **66**, 055805 (2002).
- [8] C. Ugalde *et al.*, Phys. Rev. C **76**, 025802 (2007).
- [9] U. E. P. Berg, K. Ackermann, K. Bangert, C. Blsing, W. Naatz, R. Stock, K. Wienhard, M. K. Brussel, T. E. Chapuran, and B. H. Wildenthal, Phys. Lett. **B140**, 191 (1984).
- [10] R. Schwengner, A. Wagner, Y. Fujita, G. Rusev, M. Erhard, D. De Frenne, E. Grosse, A. R. Junghans, K. Kosev, and K. D. Schilling, Phys. Rev. C **79**, 037303 (2009).
- [11] C. E. Moss, Nucl. Phys. **A269**, 429 (1976).
- [12] G. M. Crawley, C. Djalali, N. Marty, M. Morlet, A. Willis, N. Anantaraman, B. A. Brown, and A. Galonsky, Phys. Rev. C **39**, 311 (1989).
- [13] H. R. Weller, M. W. Ahmed, H. Gao, W. Tornow, Y. K. Wu, M. Gai, and R. Miskimen, Prog. Part. Nucl. Phys. **62**, 257 (2009).
- [14] S. Agostinelli *et al.* (GEANT4 Collaboration), Nucl. Instrum. Methods Phys. Res. A **506**, 250 (2003).
- [15] N. Pietralla *et al.*, Phys. Rev. Lett. **88**, 012502 (2001).
- [16] L. C. Biedenharn and M. E. Rose, Rev. Mod. Phys. **25**, 729 (1953).
- [17] P. M. Endt, Nucl. Phys. **A521**, 1 (1990).
- [18] P. M. Endt, Nucl. Phys. **A633**, 1 (1998).
- [19] I. J. Kim, C. S. Park, and H. D. Choi, Appl. Radiat. Isotopes **58**, 227 (2003).
- [20] H. W. Drotleff, A. Denker, J. W. Hammer, H. Knee, S. Kuchler, D. Streit, C. Rolfs, and H. P. Trautvetter, Z. Phys. A **338**, 367 (1991).
- [21] V. Harms, K.-L. Kratz, and M. Wiescher, Phys. Rev. C **43**, 2849 (1991).
- [22] H. W. Drotleff, A. Denker, H. Knee, M. Soine, G. Wolf, J. W. Hammer, U. Greife, C. Rolfs, and H. P. Trautvetter, Astrophys. J. **414**, 735 (1993).